Multiple contact compression tests on sand particles.

M.C. Todisco[+], W. Wang[+], M.R.Coop[*] and K. Senetakis[#]

ABSTRACT

Particle crushing has been recognised to be of key importance for many engineering applications. In soil mechanics, this phenomenon has become crucial in defining a complete framework able to describe the mechanical behaviour of sands. In this study, the effect of multiple discrete contacts on the breakage of a grain was investigated, crushing coarse grains of a quartz sand and a crushed limestone sand between a number of support particles, thereby varying the number of contacts, i.e. the coordination number. The stress at failure was calculated when the particle broke, which was through a number of distinct modes, by chipping, splitting or fragmenting which were observed with the use of high speed microscope camera. The Weibull criterion was applied to calculate the probability of surviving grain crushing and the fracture modes were observed for each configuration of the supporting particles. The data showed that in addition to the number of the contacts the nature of those contacts, controlled by the particle morphology and mineralogy, play a significant role in determining the strength of a particle. The sphericity affected the strength for the softer limestone while the local roundness at the contacts was important for the harder quartz sand. Catastrophic explosive failure was more often observed in particles with harder contacts while softer contacts tended to mould relative to their neighbouring particles inducing a more frequent ductile mode of crushing.

[+] City University of Hong Kong

[*] University College London, formerly City University of Hong Kong

[#] University of New South Wales, formerly City University of Hong Kong

1. INTRODUCTION

Understanding particle crushing is very important for modelling, simulation and optimisation of mineral and powder processing (Tavares, 2007) and in soil mechanics, establishing a link between particle breakage phenomena and the macro-mechanical behaviour of sands has become of key importance (McDowell and Bolton 1998; McDowell, 2002; Coop et al., 2004; Muir Wood, 2008; Altuhafi and Coop, 2011). Failure models accounting for the coordination number, CN, in an assembly of grains have been developed by many authors, for example Tsoungui et al. (1999) and Ben-Nun and Einav (2010) among others. In an assembly of poly-dispersed granular materials, the breaking process of the soil matrix depends on the strength of each grain, which varies with their size, and on the number of contacts which is established between grains, since the forces transferred within the assembly vary with the number of contact points. Contact force networks inside an assembly of discs have been determined by the use of photo-elasticity techniques (Drescher and De Josselin de Jong, 1972; Durelli and Wu, 1984). However, it is difficult to define the stress evolution in a system of sand specimens since the photo-elasticity method cannot be applied to sand particles, although Fonseca et al. (2016) have inferred the strong force network from an analysis of particle contacts with x-ray CT. Numerical simulations have explored the stress distributions which lead to the failure of an individual grain subjected to a system of forces within an assembly (Ben-Nun and Einav, 2010; Minh and Cheng, 2013). Gundepudi et al. (1997) extended the solution for the stress distribution in an elastic sphere under a single contact load (Dean et al., 1952) to spheres under multiple contacts. Numerically they found that the maximum stress away from the contact region was similar for uniaxial and four-point loading on different planes of the sphere, larger for three-point in-plane loading but smaller for six contact points. However, they also observed experimentally that the failure of glass and aluminium spheres initiated in the proximity of the contacts, where the contact forces reached the maximum.

In rock engineering, the Brazilian test has been used to assess indirectly the tensile strength of brittle materials. Li and Wong (2013) reviewed the mechanism of crack initiation inside the disc of rock. They found numerically that a crack in a disc subjected to two opposing forces might originate near to the two loading points along the central axis when the tensile strain overcomes a critical tensile strain threshold, or at the centre of the contact when the tensile stress overcomes the critical tensile stress threshold. However, if a fracture initiates far from the centre of the disc, the Brazilian test is not appropriate to measure the tensile strength of rocks (Fairhurst, 1964). For point load tests on an elastic sphere, Russell and Muir Wood

(2009) gave an analytical solution that showed the initial failure would occur just below the contact point and it was of shearing type, the failure criterion being dependent on the second invariant of the stress tensor. Russell et al. (2009) applied the same failure criterion to particles subjected to multi-contact loading within several different regular packings of spheres. The failure initiated near the largest contact force, when the ratio of the second to the first invariant of the stress tensor was the largest of the localised maxima, independently of the material properties or particle size. However, the yield or failure of the assembly would depend on both the maximum contact forces and the assembly stability.

Based on CT images, Zhao et al. (2015) were able to relate the internal features of quartz and decomposed granite particles to their geological origins and to explore how these features affected their mode of crushing. The single-particle crushing tests on quartz grains showed that the crushing occurred along tensile planes roughly parallel to the loading direction, although conchoidal in shape. However, they also observed an extensive fragmentation at the contact points as also shown by Gundepudi et al. (1997), which might have been generated by shear failure, as described by Russell and Muir Wood (2009).

This experimental study is an extension of preliminary results by Todisco et al. (2015) who performed multiple but discrete contact crushing tests on 60 particles of a crushed limestone and 68 of a quartz sand from the UK. The updated testing programme comprises 362 and 233 tests on quartz and crushed limestone, respectively, the much larger number of tests allowing a much clearer assessment of the factors affecting the breakage. The data were interpreted in terms of nominal stresses, i.e. characteristic stresses, which might not reproduce accurately the real stress distributions within particles under compressive loads but they offer the basis for a statistical comparison between the different types of compressive loading. Specimens were tested varying the number of contact forces on the particles, i.e. the coordination number, CN. The stress at failure was calculated when the particle broke, which was through a number of distinct modes, by chipping, splitting or fragmenting. The Weibull criterion (Weibull, 1951) was applied to calculate the probability of surviving grain crushing and the influences of the particle morphology and mineralogy on failure were investigated.

2. MATERIALS, EQUIPMENT AND TESTING PROCEDURES

The crushing tests were performed at a constant rate of 0.1 mm/min in a modified CBR apparatus equipped with a high speed camera with a microscope lens of maximum magnification of 16x (Fig. 1). The fastest frame rate of the camera was 2130 frames/sec, however tests were conducted at 1000 frames/sec because this gave the best compromise between capturing time and exposure and so the best picture quality (Wang and Coop, 2016). The forces and displacements were measured with a load cell of 1000 N capacity and 0.1 N resolution and an LVDT of ±3.5 mm linear range and 1μm resolution. The crushed particle, No.1 on Fig. 2, was placed in between others, which in turn were glued onto steel mounts using epoxy resin. The mounts were fixed into brass wells; the lower of the two was fixed to an aluminium platen which in turn was placed onto ball bearings in order to release the lateral restraint and ensure that the exact number of loading contacts occurred between the crushed particle and the others.

Wang and Coop (2016) investigated single particle crushing also using high speed photography, but here the aim of the work was to investigate the effects of the number and nature of the contacts. This photographic technique allows much larger numbers of particles to be tested than CT scanning, so that strength distributions may be determined. The tests were performed in three different configurations, varying the number of the contacts, CN, between the crushed particle and the others. The three different modes of the tests are described in Fig. 2. When the particle is crushed in between two hardened steel mounts, the test is the standard single particle crushing test (Nakata et al., 1999); when the particle is crushed between three particles at the bottom and one at the top, the test defines a multi-particle crushing test with CN equal to 4, while, when there are three particles at both the bottom and the top, the multi-particle crushing test has a CN equal to 6. It is emphasised that in the SP test an irregular sand particle has at least three points of contact if at rest on a horizontal plane and four if is crushed between flat surfaces. However, the configurations SP and CN4 of this paper are likely to be different because the contacts of the former would be in closer proximity. The single particle crushing tests have therefore been identified with SP. The differences of strength between the two types of test will be discussed below. The test configurations used are the only ones available for which the number of contacts can be ensured. While Russell et al. (2009) could investigate numerically the behaviour of particles within regular arrays of perfect equal sized spheres, these packings cannot be used in experimental work on real particles.

The coordination number, CN, and the type of support particles (steel balls, BP, or sand particles, PP) define the type of test. For example, CN4-BP refers to a test with steel ball support particles and a coordination number of 4. If sand particles were used for the support, they were always of the same size and mineralogy as that being crushed. It was rare that significant damage occurred to the support particles, and for the few occasions where it did happen the tests were discarded.

The crushing mechanism was investigated for two types of sands. The first material was the Leighton Buzzard sand (LBS), a quartz sand from the UK extensively studied in the geotechnical field since the early 70s (Stroud, 1971). The second sand was a crushed limestone (LMS) from China made of weak and angular calcite particles. The crushed limestone is a diagenetic rock, consolidated (compressed) to large stress levels and so is unlikely to have significant intra-particle voids or internal defects, as, for example, biogenic sands or weathered soils would show. Zhao et al. (2015) made CT scans of the LBS and also highly decomposed granite (HDG) particles to relate the initial microstructure to the fracture mechanism. The LBS particles only showed very few internal voids which did not influence the fracture pattern and the particles crushed with conchoidal fractures, as expected in quartz. In contrast, the complex initial microstructure of HDG, with intra-particle fissures, phase boundaries between different minerals and cleavage in some of those minerals, meant that the fracture patterns were dominated by the internal particle structure, with the coexistence of bending, shear and tensile cracks along different features. Wang and Coop (2016) also used decomposed granite and the LBS in their single particle tests. However, the complexity of the internal structure of the decomposed granite revealed by Zhao et al. meant that it was less suitable for the current study that was aimed at investigating the influence on breakage of the nature and number of contacts, which was why the crushed limestone was chosen instead as the second, softer and weaker material.

The three descriptor diameters were defined for the particles in their at-rest position as the maximum and intermediate Feret diameters in the horizontal plane and the minimum in the vertical, measuring each with a Vernier calliper of 0.01 mm resolution. The use of a Vernier calliper was preferred to a digital image method for the measurements of the particle dimensions because it allowed the characterisation of the large number of specimens required for the statistical analysis in a relatively short time but without jeopardising the measurement accuracy. The average of the minimum diameter, i.e. the thickness of the particle, was around 2.20 mm for both the sands. The descriptor diameters along with the shape characteristics and the global hardness of the materials are indicated in Table 1. The shape descriptors were evaluated as sphericity, S, and roundness, although in this study, it was preferred to use a local roundness parameter, in terms of the geometry of the grains at the contact rather than the global roundness of the grains. The sphericity, S, was calculated from the two vertical side views as the ratio between the radii of the maximum inscribed and the minimum circumscribed circles defined from the outline of the particle (Krumbein and Sloss, 1963). The side views were obtained from high quality images in two orthogonal directions. The formula, which accounts for the average sphericity from both side views, is given in Eq. 1:

$$S = \sqrt{S_A S_B} = \sqrt{\frac{r_{max,inc,A}}{r_{min,circ,A}} \cdot \frac{r_{max,inc,B}}{r_{min,circ,B}}} \tag{1}$$

where A and B refer to the different side views, S is the sphericity, $r_{max,inc}$ is the maximum inscribed radius and $r_{min,circ}$ is the minimum circumscribed radius.

A new parameter, named relative local roundness, r_{rl}, was defined to quantify the local outlines of two particles at their contacts. An image processing technique was used both in the quantification of this and the sphericity. The pictures of the particles were first transformed into a binary format and then, for r_{rl}, a polynomial function $f(x)$ of the fifth order was used to fit the outline of the binary image using Matlab. The fifth order function was the best fit of the particle outlines. Fig. 3 shows a comparison between a typical particle outline and the fitting quality of the polynomial functions of different orders. At the high magnification shown, the pixel size of the captured image is evident but it is clear that functions of lower degrees are too inaccurate to characterise the local curvature, while the sixth order did not show a better accuracy. The whole particle perimeter was divided in two parts so that the digitised outline was only a function of one independent variable (x). The radius of curvature $r_i(x)$ of one contact point was calculated according to the general formula for the curvature, χ, of a given function, $f(x)$:

$$\chi = \frac{1}{r_i(x)} = \frac{|f(x)''|}{(1+(f(x)')^2)^{3/2}} \tag{2}$$

where $f(x)$ is the function at the point (x) selected on the contact surfaces. The radius of curvature of each particle r_j was calculated as the average of $r_i(x)$ along the whole contact region:

$$r_j = \sum_{i=1}^{N} \frac{r_i(x)}{N} \tag{3}$$

where N is the number of points that defined the function *f*(x) along the contact region. Since the test configuration meant that the crushed particle was in contact with others, a measure of the geometry for each contact was established as follows (Eq. 4):

$$r_{1,j} = \frac{r_1 r_j}{r_1 + r_j} \quad (4)$$

where 1 refers to the crushed particle and j to the j-th particle which was in contact with particle 1. The r_{rl} was then defined as the minimum $r_{1,j}$ divided by the thickness of the crushed particle, $d_{1,min}$, in order to create a parameter independent of the particle size (Eq. 5). The procedure for the calculation of the shape descriptors is shown in detail in Fig. 4, where the functions *f*(x) are schematised as arcs and only three views are presented for simplicity (arcs were not used in the actual calculations).

$$r_{rl} = \frac{\min(r_{1,j})}{d_{1,min}} \quad (5)$$

The calculation of r_{rl} may be conducted in 2-D or 3-D. In 3-D, the contacts were not assessed only from the front view but different orientations were considered in order to give the optimum and complete view of the contacts. For example, generally, five pictures were taken for each CN4 configuration (three at the bottom and two at the top). Wang and Coop (2016) conducted only single-particle crushing tests, but demonstrated that there was no significant difference between using a 2-D or 3-D parameter. Ideally the contact geometry could be quantified most accurately using CT scanning, (e.g. Fonseca et al., 2013), but it would be impractical to scan a sufficient number of tests to be able to establish the characteristic stress:survival probability curves.

The high-speed camera was used to record the crushing process during the test. The videos were post-processed in order to locate the initiation of the failure crack within the particle and characterize the crushing mechanism. The Weibull criterion was applied to the data analysis and the failure stresses were obtained from Eq. 6, which assumes a tensile failure:

$$\sigma_f = \frac{F}{\pi\left(\frac{d_{int}}{2}\right)\left(\frac{d_{min}}{2}\right)} \quad (6)$$

where F is the maximum force recorded from the test, and d_{int} and d_{min} are the intermediate and minimum diameters of the crushed particle, respectively. Considering the failure area of the particle as the geometric mean of the d_{int} and d_{min} diameters would allow the effect of the particle morphology to be accounted for, especially in the case of the elongated particles. An example of the effect of the failure area on the particle strength is shown in Fig. 5 where three different survival probabilities obtained from the geometric mean area (present study), the circle area (Nakata et al., 1999) and the circle area increased by a factor of 1.1, as adopted by Hiramatsu and Oka (1966), are compared. The use of Eq. 6 implies a simplistic stress regime within the particles at failure that is undoubtedly far from reality, particularly for the CN4 and CN6 tests, yet it is probably preferable as a means of comparison to using the failure forces, although the conclusions would be the same whether the analysis was in terms of force or stress. The calculation of the characteristic stress is based on the total force acting on the system, which must all be transmitted through the central crushed particle, although of course the local contact forces will be lower for a higher CN.

Todisco et al. (2015) observed different contact behaviours between quartz and calcite grains and underlined that the hardness of particles at the contacts was an important factor in characterising the crushing mechanism. However, they based their relationship on generic mineral hardness values available in the literature. The micro-hardnesses of LBS and LMS grains have now been measured in order to describe in a more accurate way the contact properties. A Fisherscope HM2000XYp was used on fresh particle surfaces with an indentation force of 1N for both the materials. Polishing and grinding the particle surfaces were avoided since these actions may affect the residual stress state and so the hardness (Griepentrog et al., 2002). The micro-hardness values reported in Table 1 refer to Martens hardness (HM) which is the ratio between the maximum specified force F and the surface area A(h) of the Vickers indenter penetrating from the zero-point of the contact:

$$HM = \frac{F}{A(h)} = \frac{F}{h^2 \frac{4sin(\frac{\alpha}{2})}{cos^2(\frac{\alpha}{2})}} \quad (7)$$

where α is the angle between the two opposite faces of the Vickers indenter and h is the depth of the indentation. Several specimens of LBS and LMS were glued with resin epoxy on to a steel mount and by means of a microscope, the flattest surfaces of each were indented at three different locations. The average value of HM for the LBS grains was equal to 6.2 GPa and of LMS 1.6 GPa.

3. RESULTS

Weibull statistics are presented for both the LMS and LBS particles along with the m-moduli, but the effect of the geometry of the contacts on the crushing mechanism is examined only for the LBS particles. It was not possible to calculate the local relative roundness of the LMS particles due to the geometry of the contacts, which often consisted of flat-to-flat surfaces (Fig. 6). In contrast, accurate values of r_{rl} could be calculated from the geometry of the contacts of the LBS particles. The total number of tests and the number of those used for the study of morphology are indicated in Table 2. Within the study of the effects of morphology, those tests that showed incipient cracks at the top of the crushed particle and also the number of tests that have not been considered in a more detailed analysis of morphology are highlighted.

3.1 Effects of the particle morphology and hardness

In order to take into account the particle sphericity, the tests on the LMS particles were divided into two groups. The first group was used to determine the probability of survival of particles characterised by values of sphericity ranging between 0.5 and 0.7, while the second probability curve was generated for the more spherical particles. Similar trends could be identified for both the CN4-PP and CN6-PP tests as presented in Fig. 7, where the more spherical particles appear to be generally weaker. However, for very weak particles (σ_f less than 10MPa) the trend is reversed. Unland and Al-Khasawneh (2009) investigated the influence of the shape of limestone particles in impact crushing tests and they found that less spherical particles were stronger.

The same selection was applied to the LBS specimens, for which the sphericity ranges chosen were between 0.4-0.6 or 0.6-0.8 for the CN4 tests and 0.5-0.7 or 0.7-0.9 for the CN6. In contrast to the LMS behaviour, the data for the LBS particles show that the sphericity has no clear effect on the failure stress, as shown in Fig. 8. For the LBS the effect of the relative local roundness at the contacts, r_{rl}, was evaluated by dividing the data into three groups of r_{rl} = 0.2-0.4, 0.4-0.5 and 0.5-0.7. The results show that particles with lower r_{rl}, i.e. sharper contacts, are weaker than particles showing more rounded contact geometries (Fig. 9).

It might be inferred that for stronger particles, like the LBS, the geometry of the contacts dominates the crushing mechanism, obscuring the effect of the overall particle shape. When the contacts are sharp, i.e. lower r_{rl}, the particle experiences large stress concentrations at the contacts which may lead to a crack initiation in the proximity of the sharp contact before the stresses can redistribute inside the whole particle. On the contrary, soft particles do not experience any stress concentration at the contacts because they mould relative to the neighbouring particles and so the whole particle participates in the crushing process. An example of this inference is shown for the LMS in Fig. 10 where, as loading proceeds, the displacements are large, but there is no evident overall failure initially, and instead it seems that the contacts deform substantially, to the point where the central particle starts to be obscured. This phenomenon must be associated more with the hardness of the limestone than its stiffness since the Young's modulus of calcite is 73–84 GPa, while that of quartz is only slightly higher at 94–98 GPa (Mavko et al., 1998; Jaeger et al., 2007).

The influence of sphericity on the crushing of the LMS particles contradicts the work of Hiramatsu and Oka (1966) who found, both by means of photo-elasticity and experiments, that the stress field inside an irregular piece of rock may be considered as the same as that within a sphere and that the tensile stress in the rock, subjected to a pair of opposing forces, agreed well with that calculated for a sphere if the latter were reduced by a factor of 0.9.

In Fig. 11, the failure stress of LMS is related to that of LBS for the test configurations of CN6-PP and CN4-PP. Each data point represents the failure stress selected at the same survival probability value on the curves of LMS and LBS respectively, so that lower values of stress describe higher probabilities of survival. The gradient of this relationship is 0.30, which is similar to the ratio of the micro-hardnesses of the LBS and LMS particles. This result suggests that the micro-hardness may play a significant role through the deformation of the contacts.

3.2 Effect of the support particles

In Fig. 12, the survival probability curves for the CN6 configuration for the LBS clearly show that the particles crushed between steel balls are stronger than those crushed between particles but no significant difference can be observed between the two types for the CN4 configuration. On the other hand, the LMS particles give similar survival probabilities for all the test configurations, as presented in Fig. 13. Indeed, the maximum variation between the characteristic stresses at a survival probability of 37% for LMS particles crushed in SP, CN4-BP and CN6-BP configurations was only 1 MPa. A small number of tests were also carried out on smaller particles which show larger failure stresses than the larger particles, as expected (Nakata et al., 1999).

This dissimilarity may be attributed to the different natures of the contacts which are established between strong and soft particles. The geometry of the contacts of a quartz particle is preserved during the test and at the contacts large stress concentrations might occur as they transfer the load without changing their morphology significantly. When a quartz grain is compressed between 6 steel balls, each contact experiences less stress concentration than during loading between 4 or 2 points. On the other hand, the soft contacts of an LMS grain do not preserve their geometry during loading, moulding relative to the neighbouring contacts, hence the stress distribution may vary much less when the LMS grain is crushed between hard (steel balls) or soft (LMS particles) materials.

3.3 Effect of coordination number

The force-displacement curves of uniaxial compression tests (SP) and particle to particle tests (CN4 and CN6) for LBS and LMS are presented in Fig. 14 (the data for LMS are redrawn from Todisco et al., 2015). Test LBS-CN6-PP shows some stick-slip behaviour due to some small movement at the particle contacts. Generally, the increase of coordination number did not change the crushing behaviour of the quartz and limestone particles, as seen in these figures, or the failure mechanisms. The LBS particles showed brittle failure (the curves are monotonic and the displacements are small) with the development of conchoidal fractures, whereas the LMS particles failed in a ductile way reaching larger displacements and showing a saw-tooth shaped curve. It might be expected that the failure force should increase with the increase of the coordination number, and Fig. 14 already shows an example of this variation. For the LBS grains, the CN6 configuration leads to a larger failure force than CN4 or SP which are quite similar. This suggests that the location of the applied loads does not influence the particle strength for SP and CN4. The effect of the coordination number on the failure force of the LMS particles in Fig. 14 is less pronounced due to the soft nature of the contacts.

In Fig. 12 the effect of coordination number is quite clear for the quartz particles which are more prone to break when subjected to diametrically opposite forces (SP) than those subjected to a more complex system of forces (CN6). At the 37% probability, the characteristic stress of particles crushed between two steel platens is generally lower (45 MPa) than that calculated for the particles crushed between other particles; for example, the characteristic stress of LBS-CN6-PP is 51 MPa and that of LBS-CN6-BP 71 MPa. The CN4 configuration does not have a clear effect on the particle strength. This might be attributed to the configuration of the loading points, where there are three contact points at the base and one at the top, which may resemble more that of a single particle crushing test since in this configuration the particle will always rest on three points at its base prior to the loading process. Therefore, it might be difficult to see a net variation between the strength obtained from the SP and CN4 tests.

For the LMS particles, as explained in Section 3.2, the effect of the coordination number is less clear, as shown in Fig. 13, although the characteristic stresses for CN6-PP tests are still slightly higher than for the other test configurations. The configuration CN4-BP overlaps that of the single particle crushing test (SP) for probabilities larger than 60%. This underlines that the location of the applied loads does not influence the particle strength also for soft particles. The factor that accounts for the variability of strength within the population of particles is the m-modulus, which is used to describe the uniformity of the strength σ of a population of grains and increases with decreasing the variability of particle strength. It generally varied from 2 to 5 for LMS and from 3.5 to 4.5 for LBS (Fig. 15), but no influence of the test configuration could be found on the m-modulus.

Simplified failure criteria developed for a disc can be used to explain why a particle subjected to diametrical forces is more prone to break than one subjected to a set of forces. Detailed explanations are given in the failure models of Tsoungui et al. (1999) and Ben-Nun and Einav (2010). When a grain is subjected to a complex state of stress, its stress condition can be reduced to the state of principal stresses in the first order, which compress the particle by the hydrostatic pressure, p, and the deviatoric stress, τ. When the tensile stress becomes greater than a threshold, a crack initiates at the disc centre and the grain fails by tensile splitting. The expression given in Eq. 8 (Tsoungui et al., 1999) implies that a grain has a higher probability of splitting when the deviatoric stress, 2τ, is much larger than the hydrostatic pressure, p, i.e. when diametrical forces act on the particle:

$$\sigma_{xx}^{0} = 2\tau - p \geq \sigma_{crit}(R) \quad (8)$$

where σ_{xx}^{0} is the tensile stress acting at the disc centre and $\sigma_{crit}(R)$ depends on the nature of the material, the dimension of the grain and the Weibull modulus, m.

Another example of a failure criterion which considers the role of the coordination number is that of Ben-Nun and Einav (2010). In their failure model of a grain subjected to isotropic loading from neighbouring grains, they considered the possibility that the crack initiates through in-plane shear fractures, i.e. mode II of Irwin's (1957) failure criteria. In this case, the authors proposed a threshold of F_{crit} equal to:

$$F_{crit} = d\sigma_{crit} f_w f_d f_{CN} \tag{9}$$

where d is the thickness of the grain, σ_{crit} is the tensile stress at failure for the largest particle, f_w is a factor accounting for particle imperfections, f_d is a factor considering the geometry of the particle at the contacts and f_{CN} is a factor accounting for the effect of the coordination number on the crushing mechanism. The expression for f_{CN}, as given by Ben-Nun and Einav (2010) and shown in Eq. 10, implies that as the coordination number increases, the factor increases leading to an increase of the critical stress threshold:

$$f_{CN} = (CN-1)e^{(D/d)(CN-2)(CN-3)/4CN} \tag{10}$$

where D is the diameter of the neighbouring particles, d is the dimension of the crushed particle and CN is the coordination number of the crushed particle. From Eq. 9, an increase of F_{crit} is reflected as a decrease of probability of failure of a grain with a higher coordination number.

3.4 Characterization of the crushing mechanism

The characteristic stresses calculated assume that the crushed particle failed in a tensile mode, obeying Griffith's criterion, for which a crack initiates in the centre of a disc when it is subjected to diametrical loads. Complete stress solutions for a grain that which fails in tension under two opposite loads acting on a finite arc have been formulated by several researchers, Hondros (1959) and Hiramatsu and Oka (1966) among others, and they are used to calculate the tensile strength of a disc of rock in the Brazilian test (Eq. 11),

$$\sigma = \frac{F}{\pi R t} \tag{11}$$

where the failure force (F) acts on the disc over an arc not greater than 10º (Li and Wong, 2013) and R and t are the radius and the thickness of the disc, respectively.

It has been argued that this formula might not be suitable for the estimation of the tensile strengths of rocks because the crack does not initiate in the centre but near the loading point (Fairhurst, 1964; Li and Wong, 2013). Recently, Russell and Muir Wood (2009) formulated a model for a point loaded sphere in which the crack initiation occurs when the ratio between the second invariant of the deviatoric stress tensor, J_2, and the first invariant of the stress tensor, I_1, is a maximum, which is essentially a maximum ratio of shear to normal stress invariants. In their work, the location of the initial failure was near the point load, at a distance between 0.7-0.9 from the centre of the sphere. In this study, this possibility was considered by eliminating the tests which showed a failure at the top for CN4 and SP tests from the data, although they were small in number as indicated in Table 2. The videos were recorded with the high speed camera and the analysis was applied only to the LBS particles tested between steel platens (SP) or 4 other particles (CN4-PP). The CN6-PP configuration was not considered because in this case the crack initiation may occur anywhere within the particle, since the forces are more equally distributed around the grain. The LMS particles were not analysed because it was difficult to determine the initiation of the failure, because the large deformations at the contacts tended to obscure the central particle.

As indicated in Table 2, out of 76 SP particles only 8 showed a failure near the top contact. Failures near the base contact were not eliminated also for SP tests because the base contact should not be unique. Of the 14 CN4-PP tests discarded, 6 showed a failure near the top contact and the remaining 8 were not taken into account because the location of the initial failure was unclear. The new probability curves shift to the right showing a small increase of particle strength (Fig. 16). This is more evident for the tests carried out in the CN4 configuration in which the characteristic stress increased from 45 MPa to 51 MPa, although a smaller number of tests was performed in comparison with the SP configuration. Any conclusion might be slightly speculative at this stage, because a large number of tests would be required to investigate whether this type of test is suitable to assess the tensile strength of the sand particles in multi-axial loading tests.

The mode of failure was also analysed through the high speed videos recorded during the tests. The two different sands behaved very differently as expected. The soft LMS crushed into many pieces in a ductile way, reaching ultimate failure by the progressive breakage of the asperities and large deformation of the contacts. Fig. 10 shows a sequence of the images captured during the video of the test and this was typical of all the tests. The crushing mode of the quartz grains was analysed for both the CN4- and CN6-PP tests. The brittle failure, common for quartz, was divided into three categories: if a grain suddenly shattered into many tiny pieces, the crushing process was classified as fragmentation, while if the grain split in two or more large parts, the crushing process was classified as splitting. It was observed that some grains failed also by the chipping of a smaller part of the particle not involving the entire particle in the crushing process (defined as “abrasion” by Tsoungui el al., 1999). Markides et al. (2010) found that discontinuities of stress and displacement fields concentrate at the edges of the load contacts and so the crack might initiate from the perimeter of the specimen. If it is made of hard material, this might not allow a smooth transition of the crack from the edge through the less loaded part and therefore the failure occurs by chipping off a piece of the specimen and not by splitting or fragmentation.

The CN4-PP specimens involved all the three crushing categories; out of the 32 tests for which a video was available, 25% failed by fragmentation, 69% by splitting and 6% by chipping (Figs. 17-19). The particles of CN6-PP failed predominantly by splitting, maintaining the two or three pieces generated from the crushing in place. An example is given in Fig. 20. The confinement given by this test configuration might cause this phenomenon. This recalls the behaviour of sand grains in triaxial tests as observed by Bandini and Coop (2011) or oedometer tests by Bolton and Cheng (2002), in which a particle that breaks while it is surrounded by others tends to create fragments that are held in close proximity to each other after failure occurs, as shown Fig. 21.

4. CONCLUSIONS

Many factors may be involved in the complex mechanisms of breakage of a sand grain. An analysis of the particle morphology and mineralogy, the nature, the geometry and the number of contacts was conducted through multi-contact compression tests on sand particles. It was found that the sphericity affects the strength for soft but not for hard materials, for which it seems to be obscured by the relative local roundness at the contacts. The more spherical of the limestone particles were stronger, and sharper contacts led to a decrease in the failure stress for quartz particles. Key importance in the crushing mechanism might be attributed to the material hardness which may affect the particle strength through the deformation of the contacts. The main difference between the crushing behaviour of quartz and calcite grains was therefore attributed to the nature of the contacts. Hard contacts preserve their morphology during loading, experiencing large stress concentrations prior to failure. Soft contacts mould relative to their neighbouring particles, involving the entire particle in the crushing mechanism.

Generally, an increase of the number of contacts induced an increase of particle stress at failure. The assumption of a tensile failure was adopted to determine the Weibull probability of the populations of sand particles, but a much larger number of tests would be needed to assess whether this approach is suitable to calculate the tensile strength of sand particles, which would be highly time-consuming for these multiple contact tests.

If the coordination number was four, either in the CN=4 or SP tests, then failure occurred by splitting, fragmenting or chipping but for CN=6 generally only splitting occurred, maintaining the products of the crushing in place.

5. ACKNOWLEDGEMENTS

The work described in this paper was fully supported by a grant from the Research Grants Council of the Hong Kong Special Administrative Region, China (Project No. CityU 112712).

6. REFERENCES

Altuhafi, F.N. and Coop, M.R., 2011. Changes to particle characteristics associated with the compression of sands. *Géotechnique*, 61(6), pp. 459-471.

Bandini, V. and Coop, M.R., 2011. The influence of particle breakage on the location of the critical state line of sands. *Soils and Foundations*, 51(4), pp. 591-600.

Ben-Nun, O. and Einav, I., 2010. The role of self-organization during confined comminution of granular materials. *Phil. Trans. R. Soc. A*, 368, pp. 231-247.

Bolton, M.D. and Cheng, Y.P., 2002. Micro-geomechanics. Lisse, Springman (ed.), pp. 59-69.

Coop, M.R., Sorensen, K.K., Bodas Freitas, T. and Georgoutsos, G., 2004. Particle breakage during shearing of a carbonate sand. *Géotechnique*, 54(3), pp. 157-163.

Dean, W.R., Sneddon, A. M. and Parsons, H.V., 1952. Distribution of stress in a decelerating elastic sphere. *Selected government research reports: Strength and testing of Materials: Part II: Testing methods and tests results , HSMO, London*, pp. 212-234.

Drescher, A. and De Josselin De Jong, G., 1972. Photoelasticity verification of a mechanical model for the flow of a granular material. *J. Mech. Phys. Solids*, 20(5), pp. 337-351.

Durelli, A.J. and Wu, D., 1984. Loads between disks in a system of discrete elements. *Experimental Mechanics*, 24(4), pp. 337-341.

Fairhurst, C., 1964. On the validity of the Brazilian test for brittle materials. *Int. J. Rock Mech. Min.*, 1, pp. 515-526.

Fonseca, J., Nadimi, S., Reyes-Aldasoro, C.C., O'Sullivan, C. and Coop, M.R., 2016. Image-based investigation into the primary fabric of stress transmitting particles in sands. *submitted to Soils and Foundations.*

Fonseca, J., O'Sullivan, C., Coop, M.R. and Lee, P.D., 2013. Quantifying the evolution of soil fabric during shearing using directional parameters. *Géotechnique*, 63(6), 487-499.

Griepentrog, M., Ullner, C., and Duck., A., 2002. Instrumented indentation test for hardness and materials parameter from millinewtons to kilonewtons. *11th IMEKO TC05 Conference on hardness measurement*, Celle, Germany, 24-26 September, pp. 53-58.

Gundepudi, M.K., Sankar, B.V., Mecholsky, J.J. and Clupper, D.C., 1997. Stress analysis of brittle spheres under multiaxial loading. *Powder Technology*, 94 (2), pp. 153-161.

Hiramatsu, Y. and Oka,Y., 1966. Determination of tensile strength of rock by compression test of an irregular test piece. *Int. J. Rock. Mech. Min*., 3, pp. 89-99.

Hondros, G., 1959. The evaluation of Poisson's ratio and the modulus of materials of a low tensile resistance by the Brazilian (indirect) test with particular reference to concrete. *Aust. J. Appl. Sci.*, 10(3), pp. 243-268.

Irwin, G., 1957. Analysis of stresses and strains near the end of a crack traversing a plate. *J. Appl. Mech.*, 24, pp. 361-364.

Jaeger, J. C., Cook, N. G. W. and Zimmerman, R., 2007. *Fundamentals of rock mechanics.* 4th ed. Oxford: Wiley-Blackwell.

Krumbein, W.C. and Sloss, L.L., 1963. Stratigraphy and sedimentation. San Francisco: W.H. Freeman and Company.

Li, D. and Wong, L.N.Y., 2013. The Brazilian disc test for rock mechanics applications: review and new insights. *Rock Mech. Rock. Eng.*, 46(2), pp. 269-287.

Markides, C.F., Pazis, D.N. and Kourkoulis, S.K., 2010. Closed full-field solutions for stresses and displacements in the Brazilian disk under distributed radial load. *Int. J. Rock Mech. Min. Sci.*, 47(2), pp. 227-237.

Mavko, G., Mukerji, T. and Dvorkin, J., 1998. *The rock physics handbook: tools for seismic analysis in porous media*. Cambridge: Cambridge University Press.

McDowell, G.R. and Bolton, M.D., 1998. On the micromechanics of crushable aggregates. *Géotechnique*, 48(5), pp. 667-679.

McDowell, G., 2002. On the yielding and plastic compression of sand. *Soils and Foundations*, 42(1), pp. 139-145.

Minh, N.H. and Cheng, Y.P., 2013. A DEM investigation of the effect of particle-size distribution on one-dimensional compression. *Géotechnique*, 63(1), pp. 44-53.

Muir Wood, D., 2008. *Critical state and soil modelling*. Amsterdam, The Netherlands, IOS Press, pp. 51-72.

Nakata, Y., Hyde, A.F.L., Hyodo, M. and Murata, H., 1999. A probabilistic approach to sand particle crushing in the triaxial test. *Géotechnique*, 49(5), pp. 567-583.

Russell, A.R. and Muir Wood, D., 2009. Point load tests and strength measurements for brittle spheres. *Int. J. Rock Mech. Min. Sci.*, 46(2), pp. 272-280.

Russell, A.R., Muir Wood, D. and Kikumoto, M. 2009. Crushing of particles in idealised granular assemblies. *J. Mech. Phys. Solids*, 57(8), pp. 1293-1313.

Stroud, M., 1971. *Sands at low stress levels in the S.S.A.*, s.l.: Cambridge University.

Tavares, L., 2007. *Breakage of single particle: quasi-static*. In: Handbook of Powder Technology-Volume 12. s.l.:Elsevier, pp. 3-68.

Todisco, M.C., Coop, M.R., Senetakis, K. and Guo, Q., 2015. The effect of coordination number on particle crushing. *Geomechanics from Macro to Micro*, *Proc. of the TC 105 ISSMGE*, IS-Cambridge 2015, Vol.2, 1063-1068.

Tsoungui, O., Vallet, D. and Charmet, J.C., 1999. Numerical model of crushing of grains inside two-dimensional granular materials. *Powder technology*, 105(1), pp. 190-198.

Unland, G. and Al-Khasawneh, Y., 2009. The influence of particle shape on parameters of impact crushing. *Minerals Engineering*, 22(3), pp. 220-228.

Wang, W. and Coop, M.R., 2016. An investigation of breakage behaviour of single sand particles using a high-speed microscope camera. *Géotechnique*, DOI: http://dx.doi.org/10.16 80/jgeot.15.P.247.

Weibull, W., 1951. A statistical distribution function of wide applicability. *Journal of applied mechanics*, pp. 293-297.

Zhao, B., Wang, J., Coop, M., R., Viggiani, G. and Jiang, M., 2015. An investigation of single sand particle fracture using X-ray micro-tomography. *Géotechnique*, 65(8), pp. 625-641.

TABLES

Table 1 Characteristics of the LBS and LMS particles (dimensions in mm, micro-hardness, HM, in GPa).

MATERIAL	d_{max}	d_{int}	d_{min}	S	r_{rl}	HM
LBS	3.61	2.90	2.21	0.63	0.48	6.2
LBS	2.62	2.15	1.62	-	-	6.2
LMS	3.46	2.70	2.24	0.69	-	1.6
LMS	2.41	1.86	1.51	-	-	1.6

Table 2 Description of the tests.

TEST CONFIGURATION	Number of tests			
	Total	Study of Morphology		
		Tests for morphology	Initiation of the crack at the top of the particle	Not considered (no video available)
LBS -SP	90	76	8	-
LBS-CN4-BP	59	-	-	-
LBS-CN6-BP	34	-	-	-
LBS-CN4-PP	70	65	6	8
LBS-CN6-PP	65	51	-	-
LBS-CN6-PPsmall	44	30	-	-
LMS -SP	28	24	-	-
LMS-CN4-BP	39	-	-	-
LMS-CN6-BP	36	22	-	-
LMS-CN4-PP	56	51	-	-
LMS-CN6-PP	58	53	-	-
LMS-CN6-BPsmall	16	-	-	-

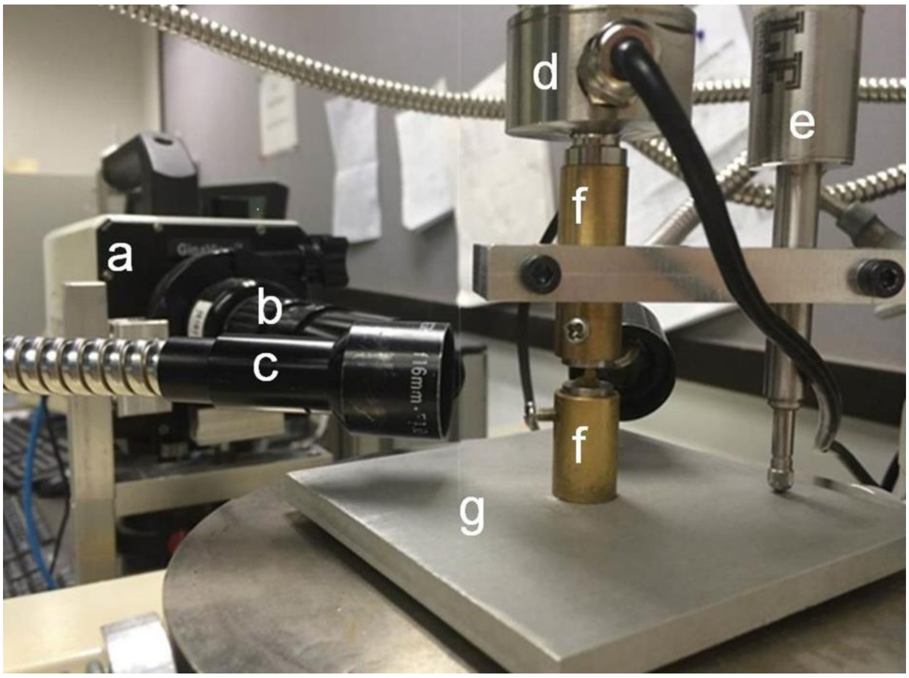

Fig. 1 Equipment for the multi-axial crushing tests: a) high speed camera; b) microscope lens; c) additional lighting system with focussing lenses; d) load cell; e) LVDT; f) brass wells containing steel mounts; g) base support resting on ball bearings.

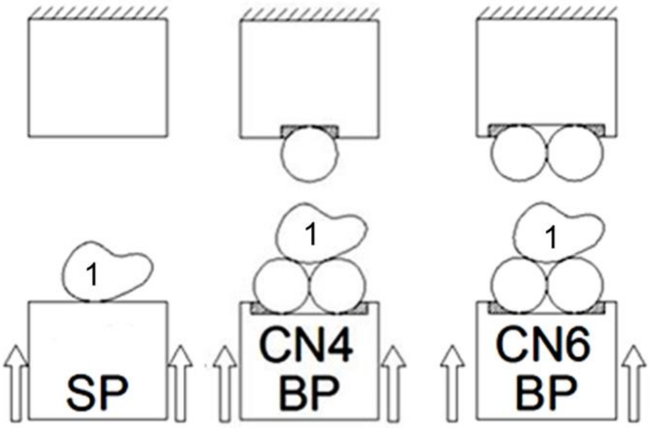

Fig. 2 Schematic representation of the multi-contacts crushing tests for particles tested between hardened steel mounts (SP), between 4 steel balls (CN4-BP) and between 6 steel balls (CN6-BP).

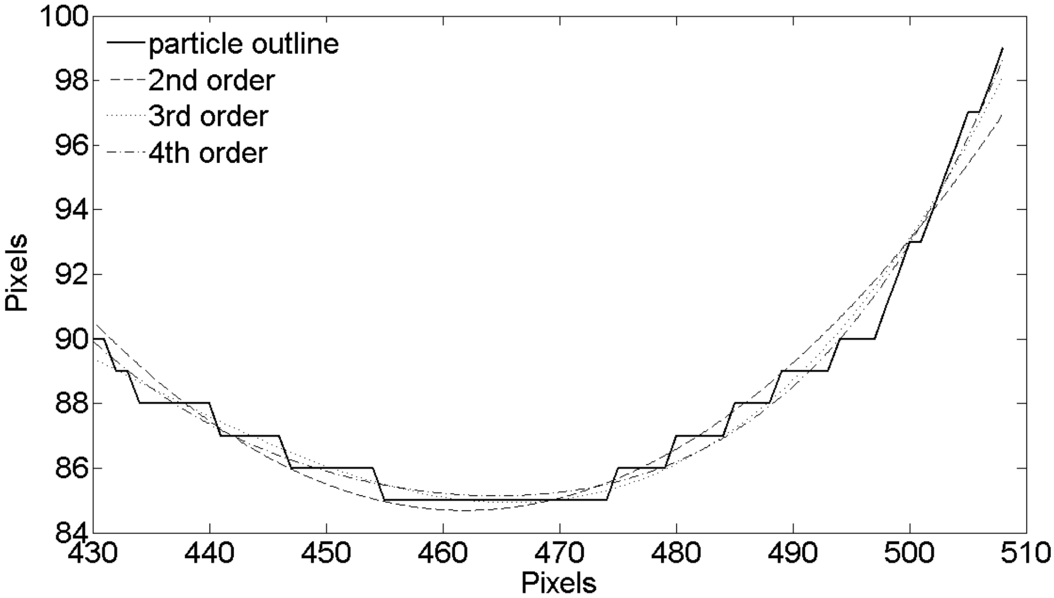

a)

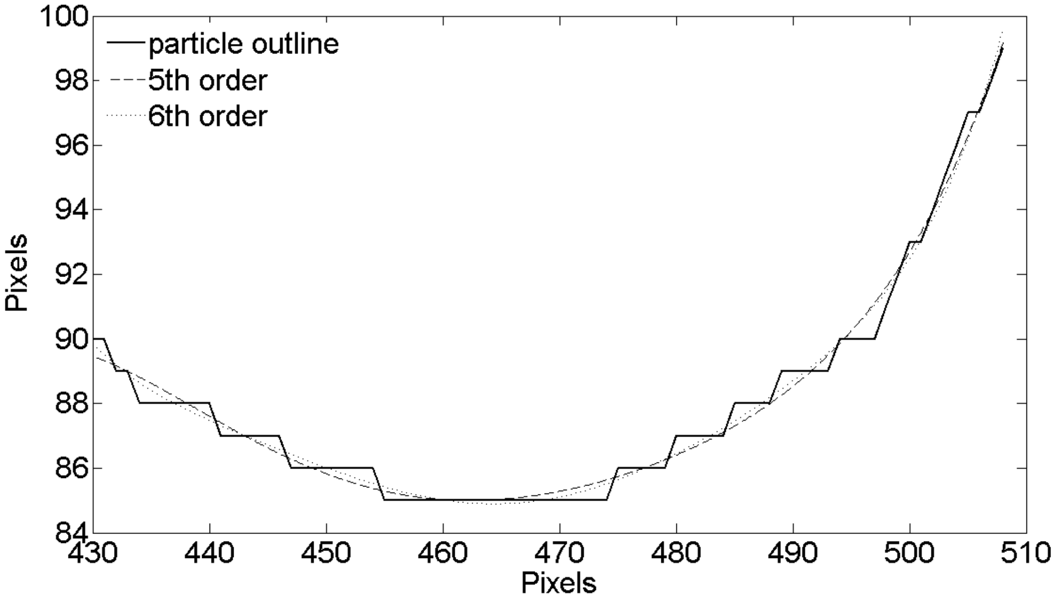

b)

Fig. 3 Fitting of a particle outline by polynomial functions of different orders: a) 2nd, 3rd and 4th orders; b) 5th and 6th orders.

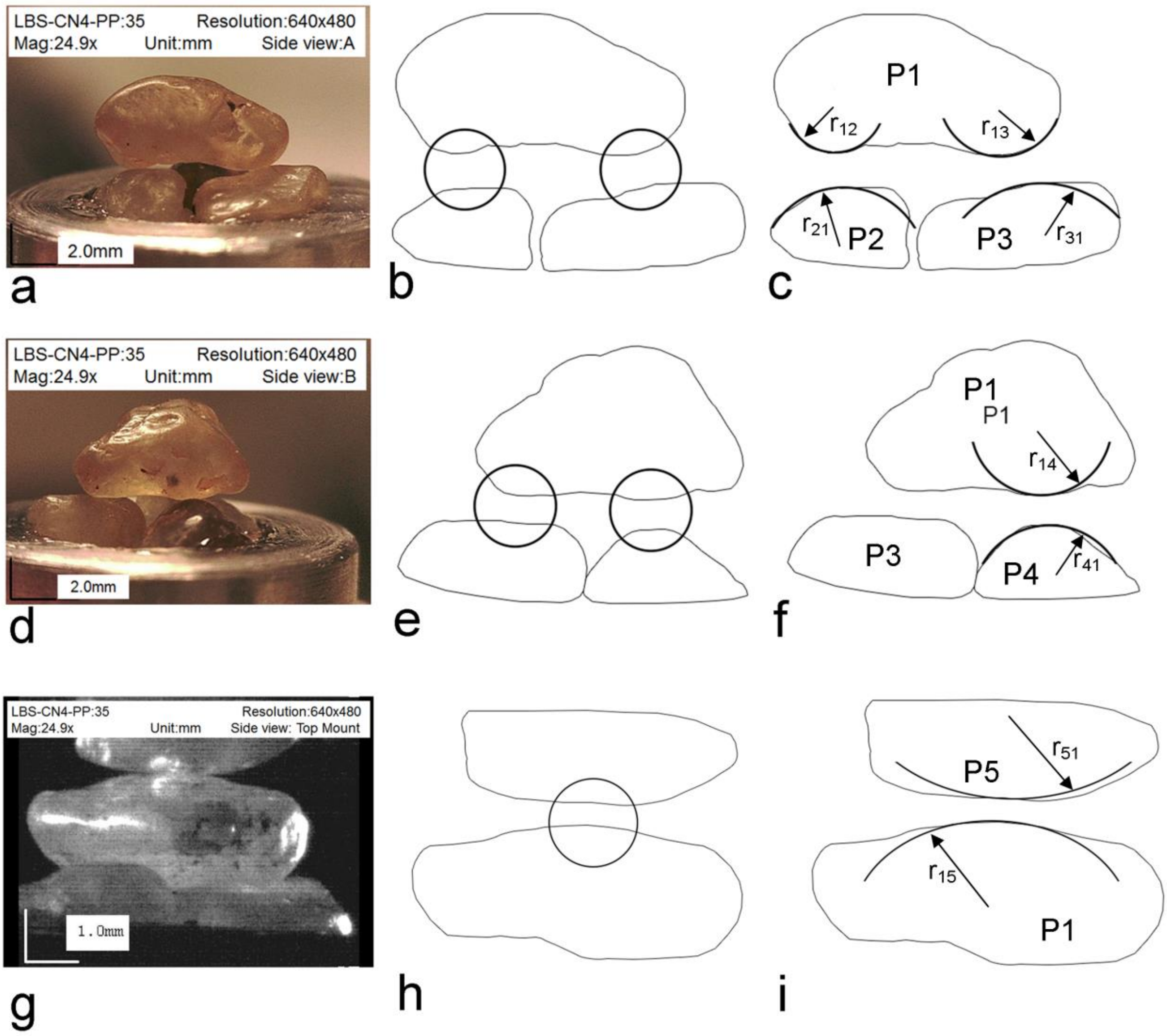

Fig. 4 Example of the local relative roundness parameter, r_{rl}, of test no.35, LBS-CN4-PP based on 3 views: a) side view A of the lower mount; b) location of the contact points of side view A; c) definition of local radius of curvature for each contact of side view A; d) side view B of the lower mount; e) location of the contact points of side view B; c) definition of local radius of curvature for each contact of side view B; g) view of top mount; h) location of the contact points at top mount; i) definition of the local radius for the contact at the top. The arrows are indicative.

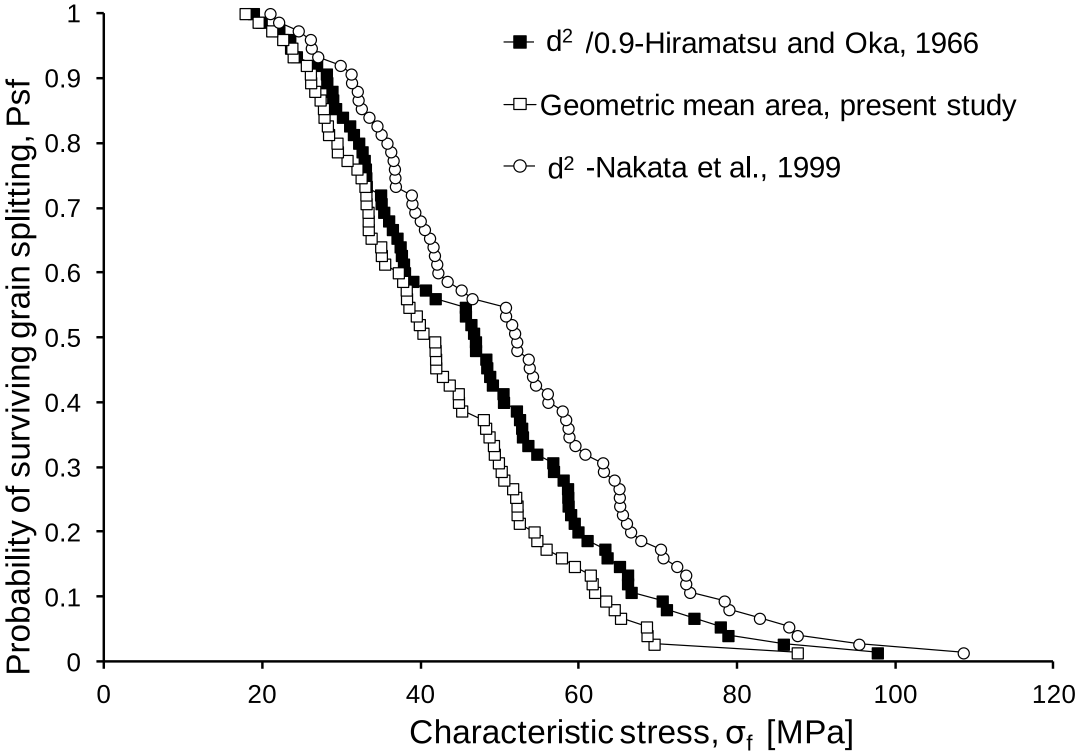

Fig. 5 The effect of the failure area on the strength of the LBS particles crushed between two hardened steel mounts, i.e. LBS- SP. The geometric mean area has been adopted in this study.

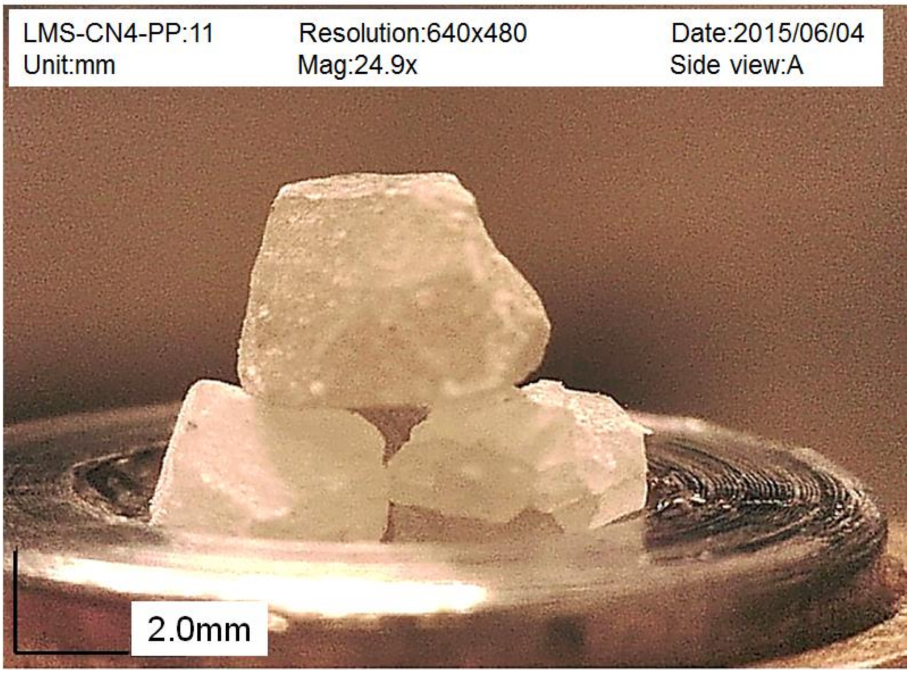

Fig. 6 Flat-to-flat contacts between LMS particles.

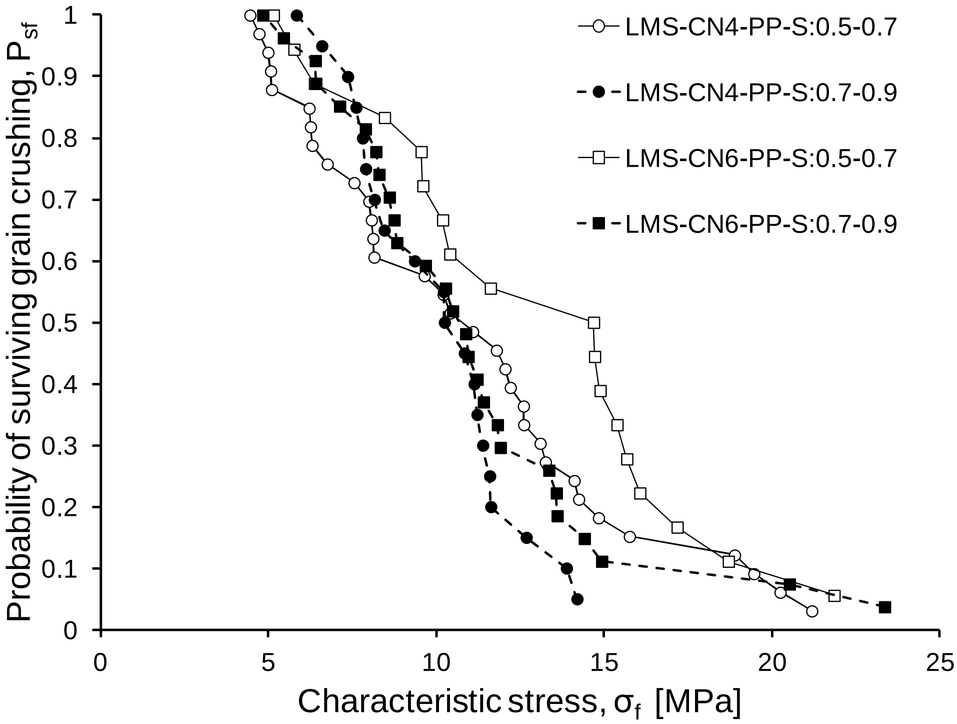

Fig. 7 The effect of sphericity on the strength of LMS particles.

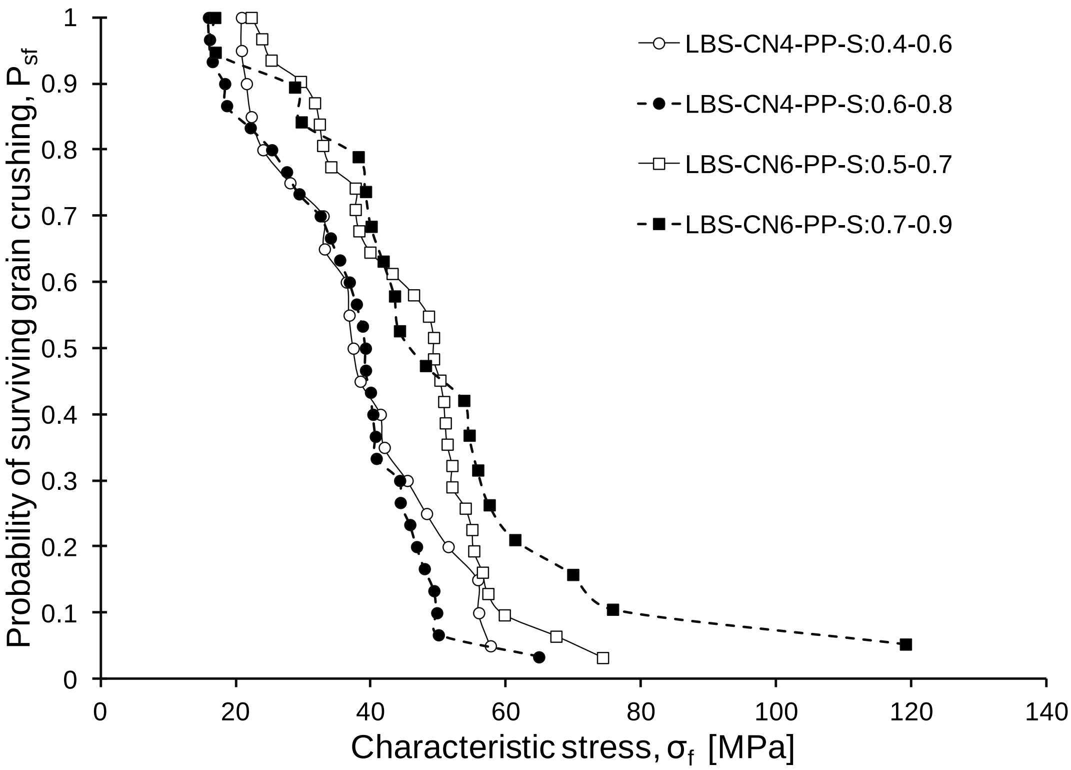

Fig. 8 The effect of sphericity on the strength of LBS particle.

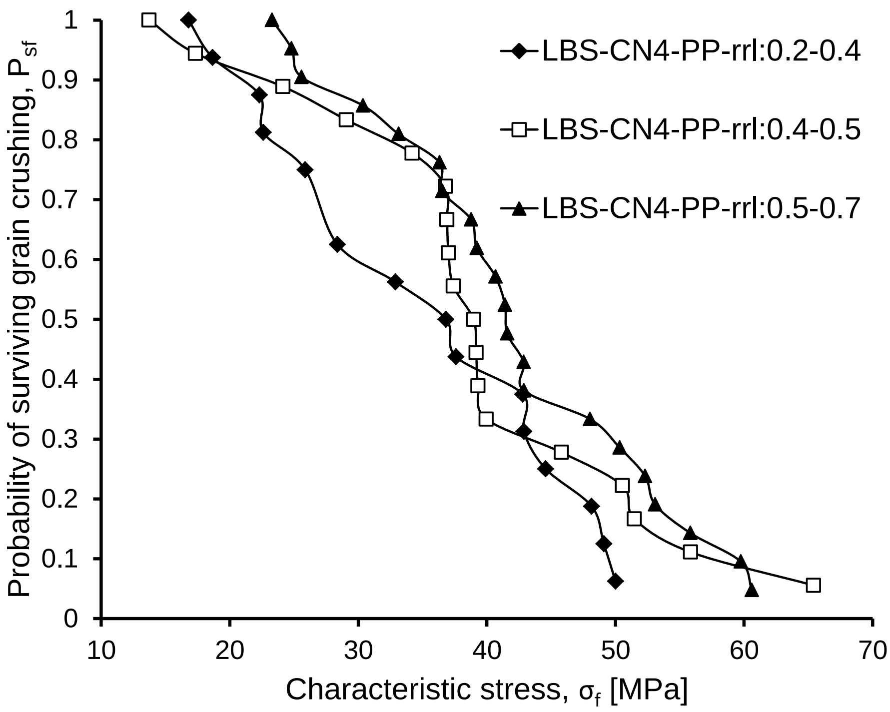

a)

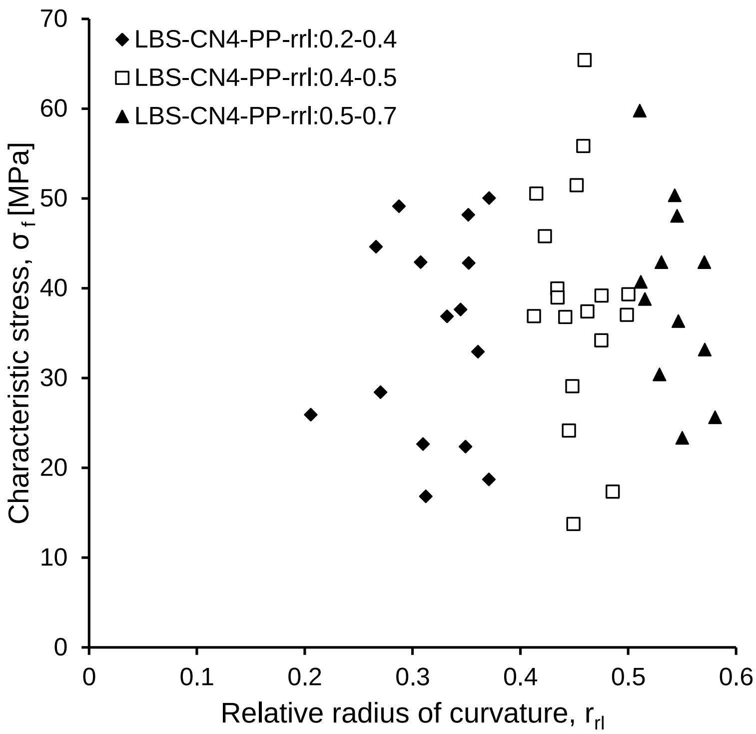

b)

Fig. 9 The effect of local roundness parameter, r_{rl}, on LBS particles: a) probability of surviving grain crushing; b) relationship between the characteristic stress and the r_{rl}.

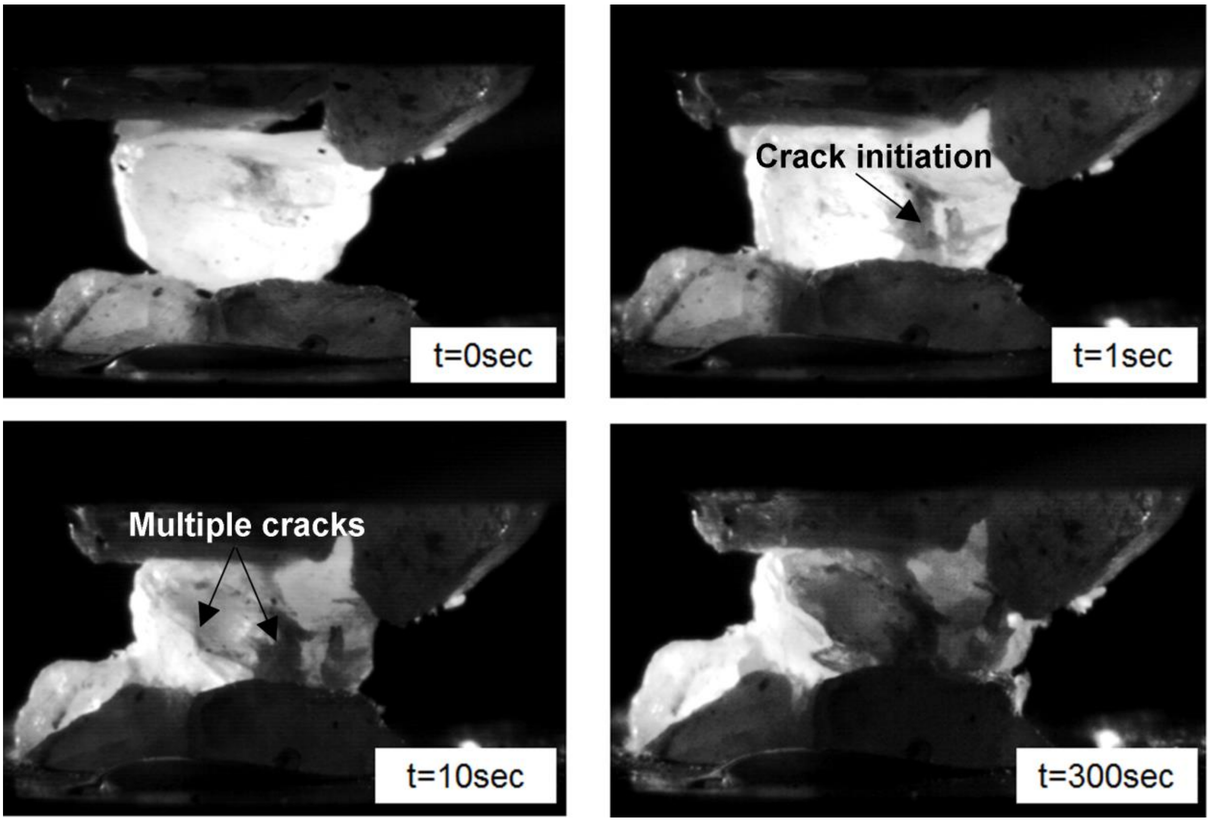

Fig.10 Example of the crushing mechanism of LMS particle tested in CN6-PP configuration.

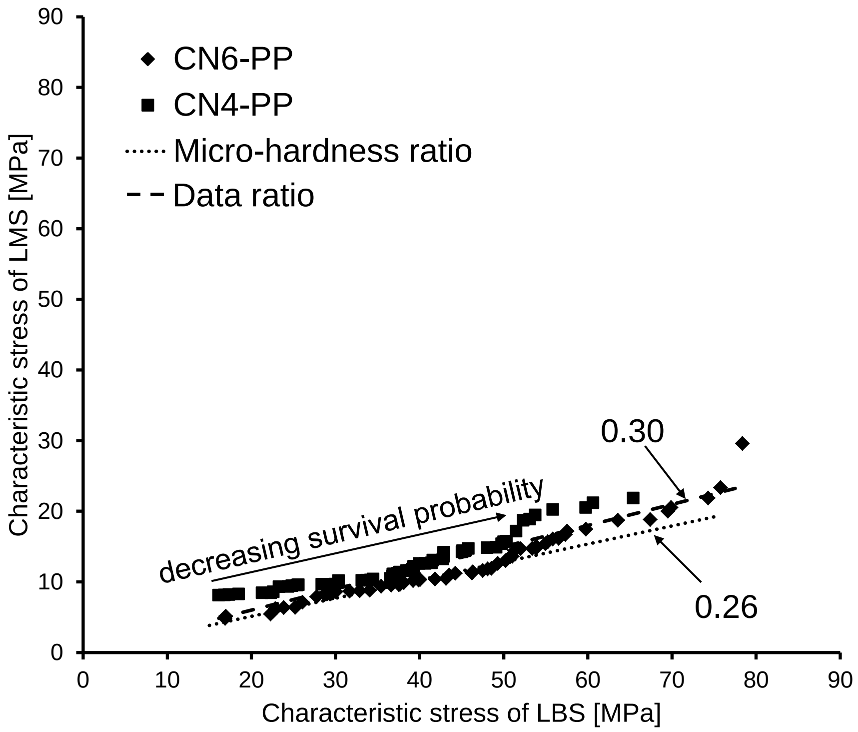

Fig. 11 Hardness relationship obtained from the characteristic stress of LBS and LMS specimens crushed in CN4-PP and CN6-PP configurations.

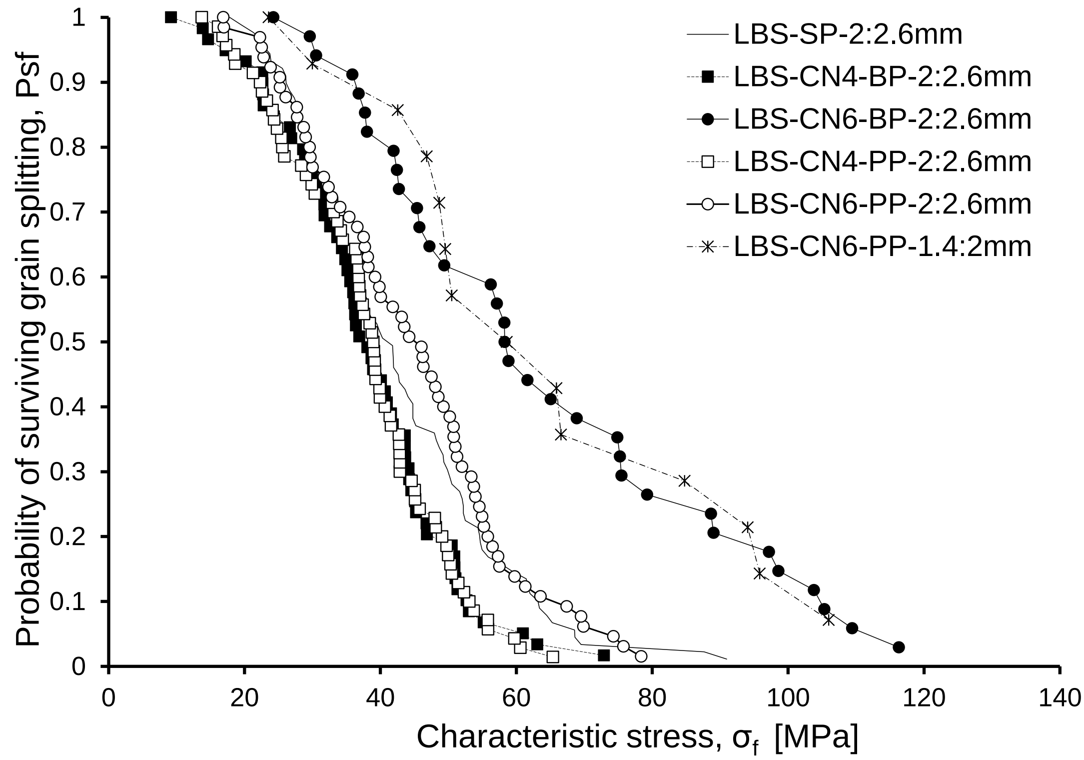

Fig. 12 Survival probability curves of LBS particles for different support particles.

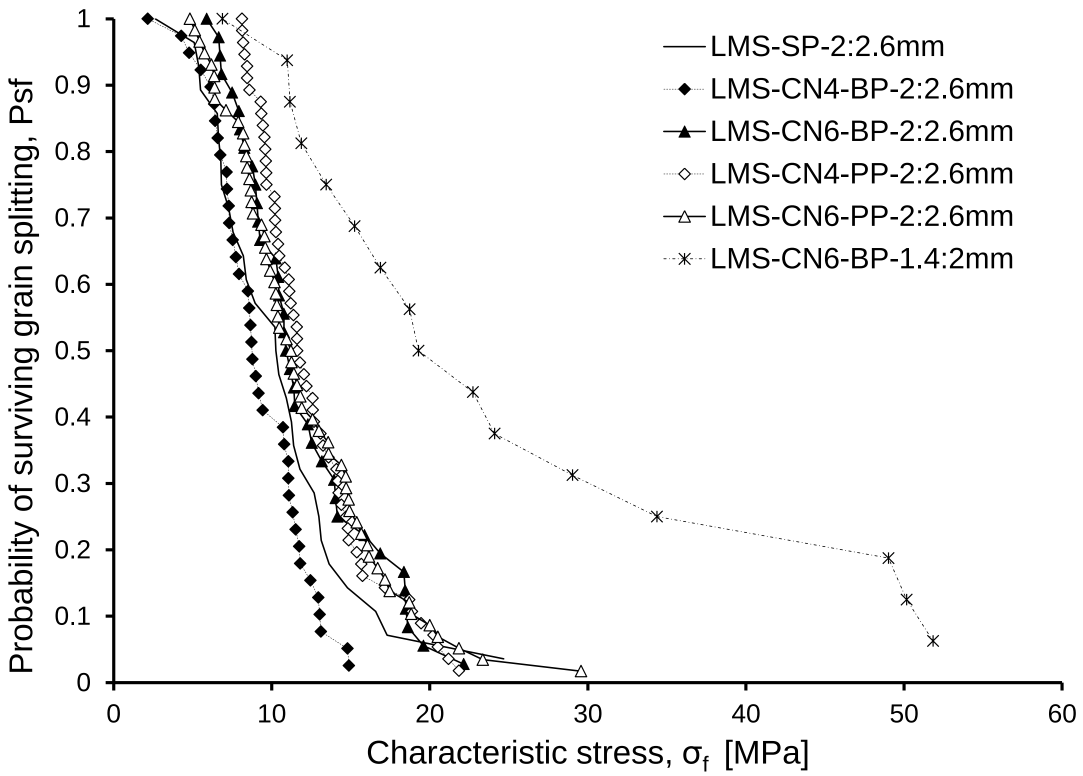

Fig. 13 Survival probability curves of LMS for different support particles.

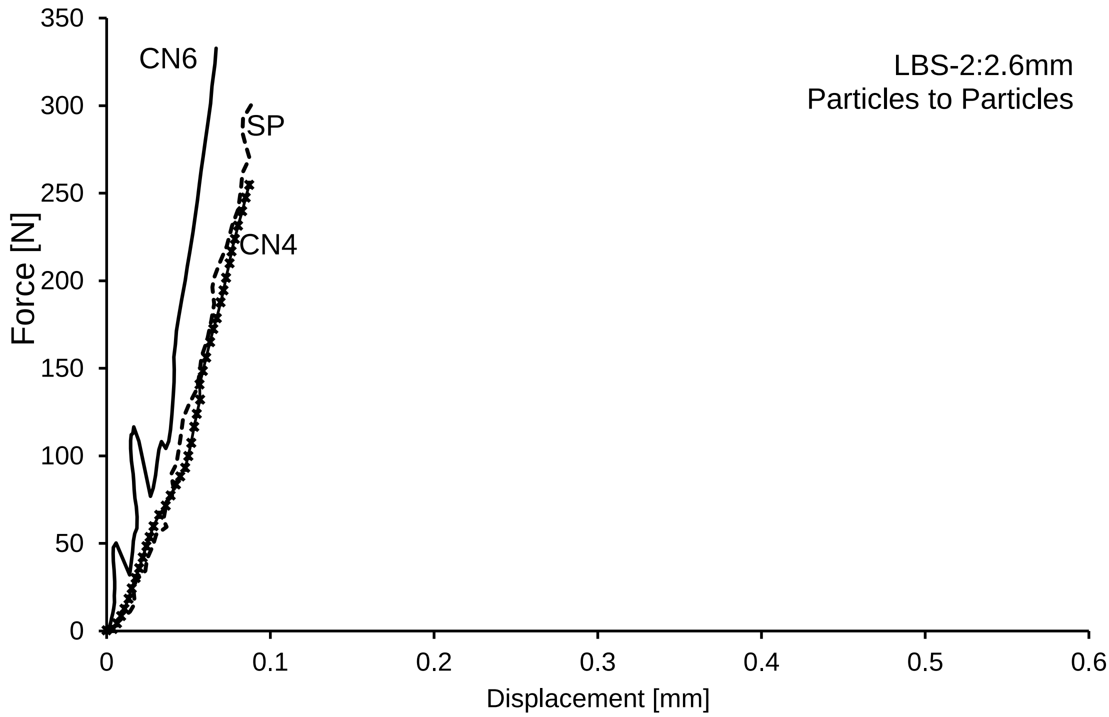

a)

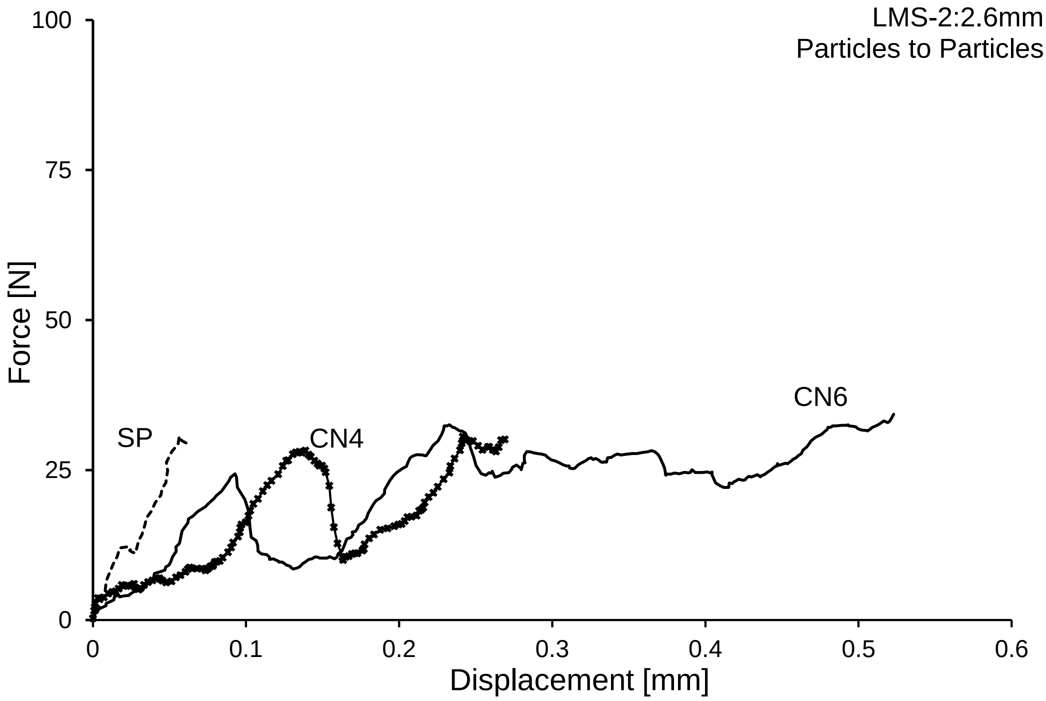

b)

Fig. 14 Force-displacement relationship of a) LBS (present study) and b) LMS (redrawn from Todisco et al., 2015) particles.

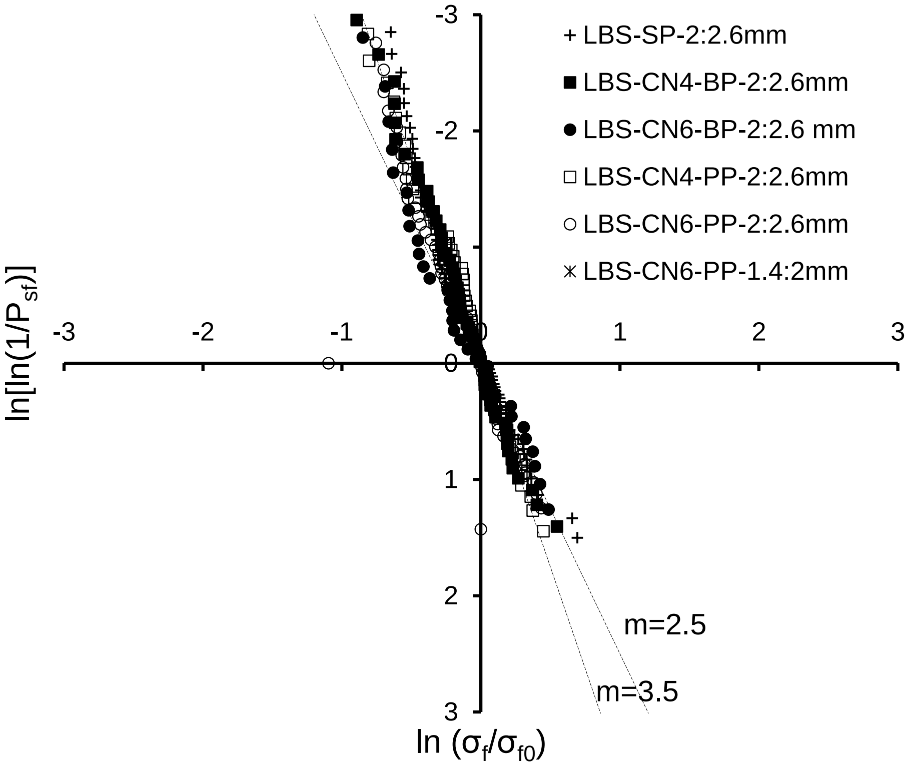

a)

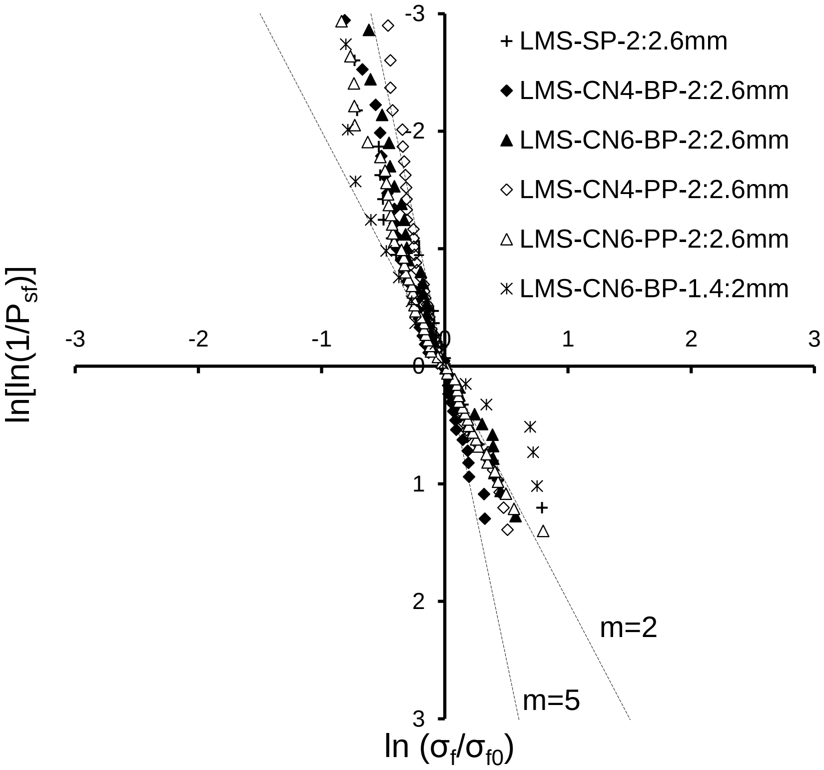

b)

Fig. 15 The m-modulus of the tested sands: a) LBS specimens; b) LMS specimens.

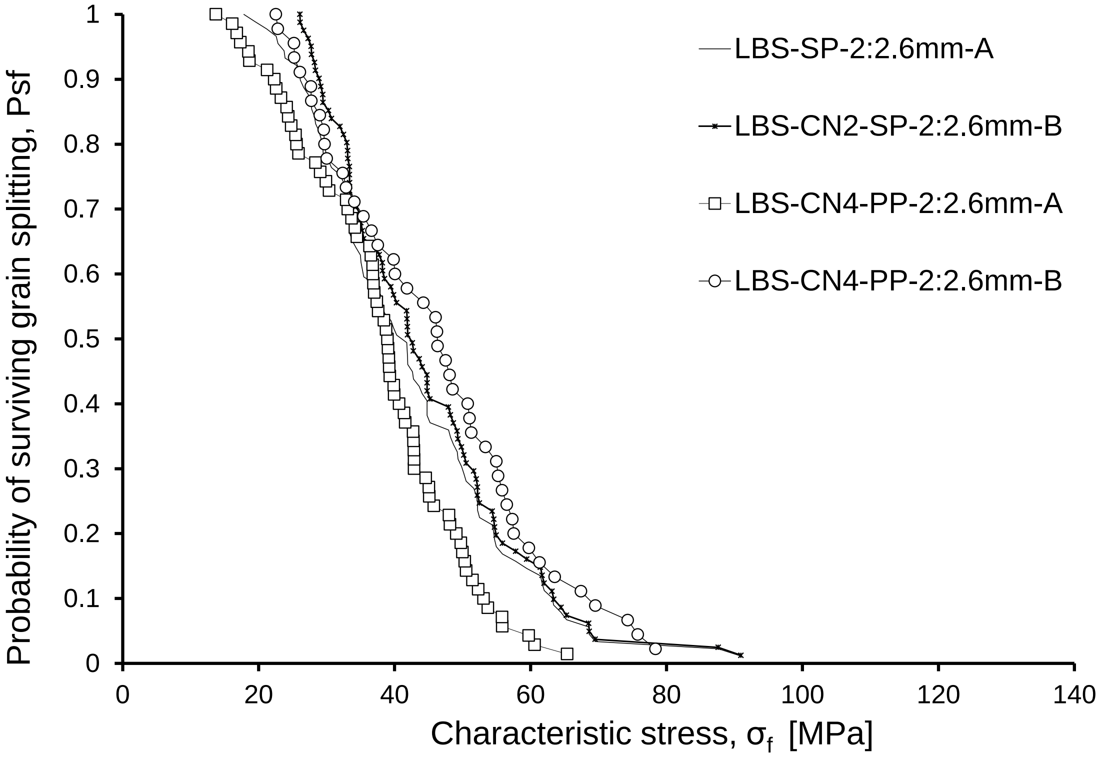

Fig. 16 Probabilities of survival of LBS particles for which the crack initiation did not occur near the top contact. The data refer to SP and CN4-PP configurations. (A all data, B with failures near top contact eliminated)

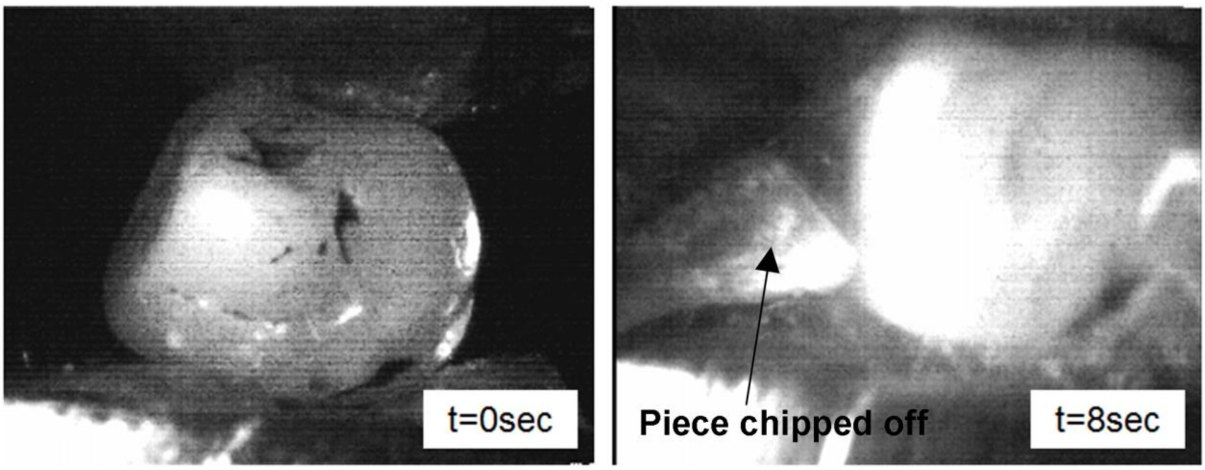

Fig. 17 Chipping crushing mechanism of LBS particle tested in between 4 particles.

632

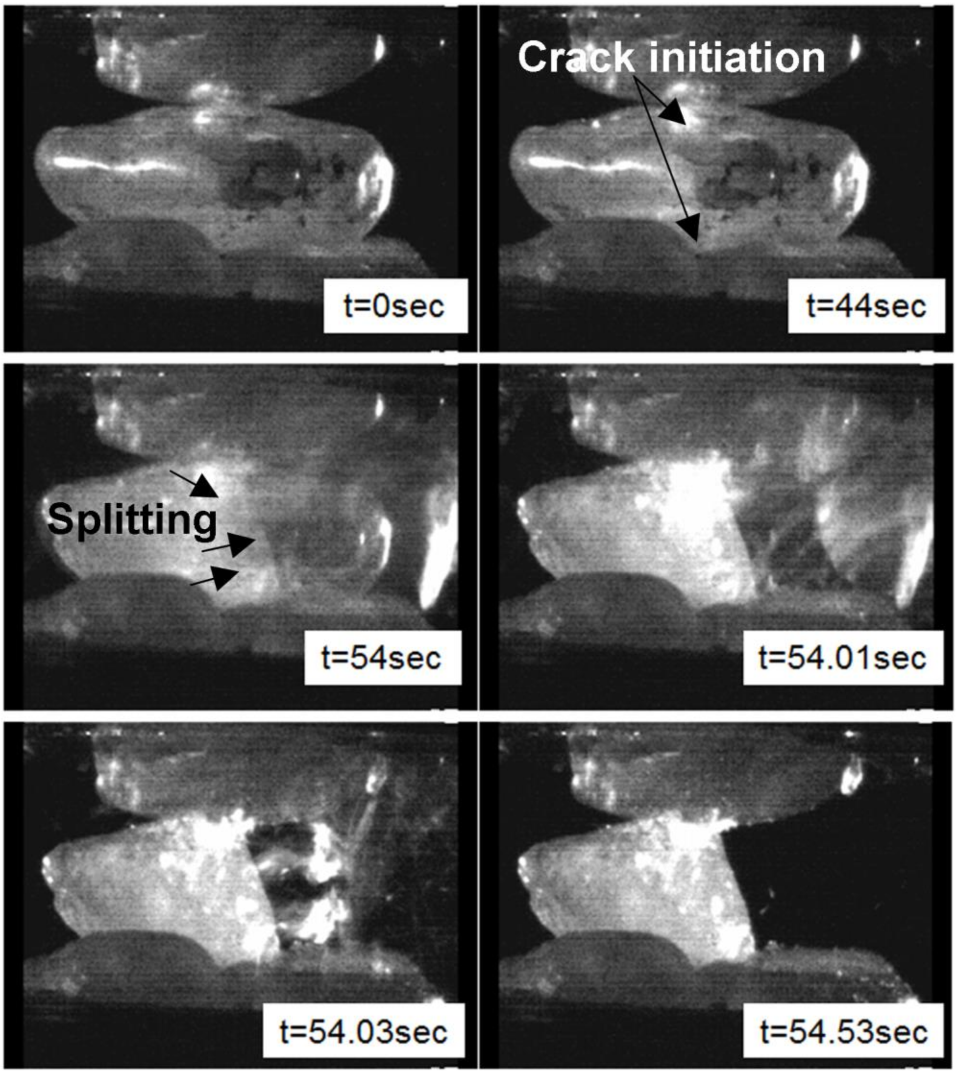

633 Fig. 18 Splitting crushing mechanism of a LBS particle tested in the CN4-PP configuration.

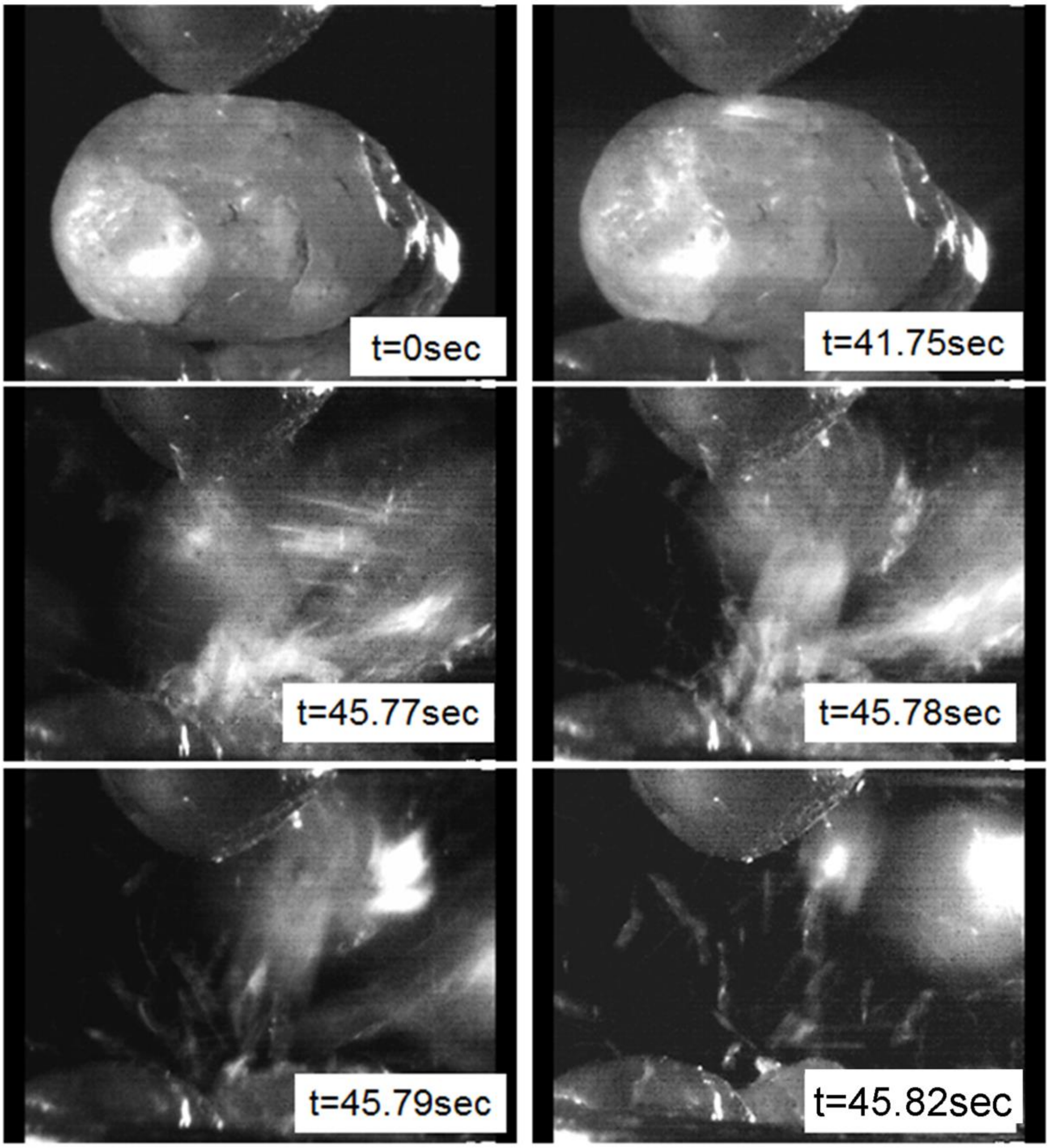

634

635 Fig. 19 Fragmentation crushing mechanism of a LBS particle crushed in between 4 particles.

636

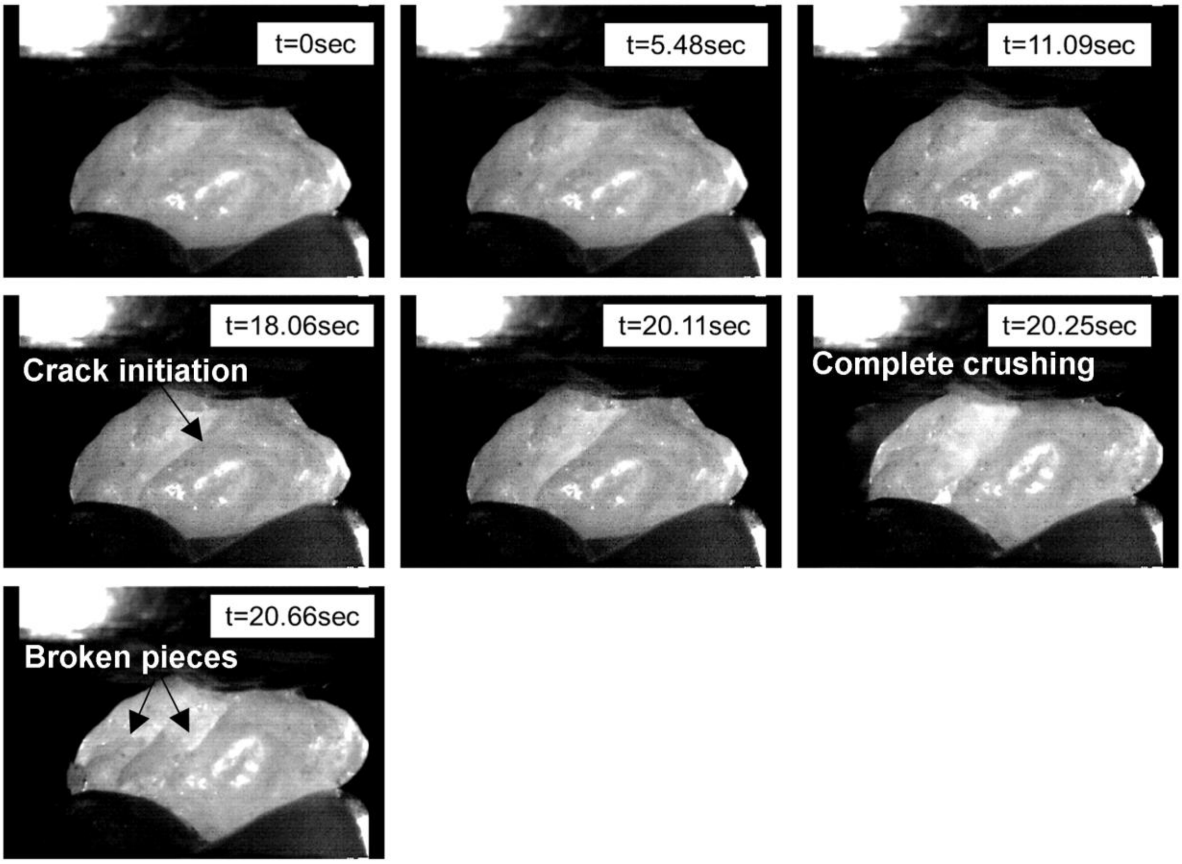

Fig. 20 Splitting crushing mechanism of a LBS particle tested in the CN6-PP configuration.

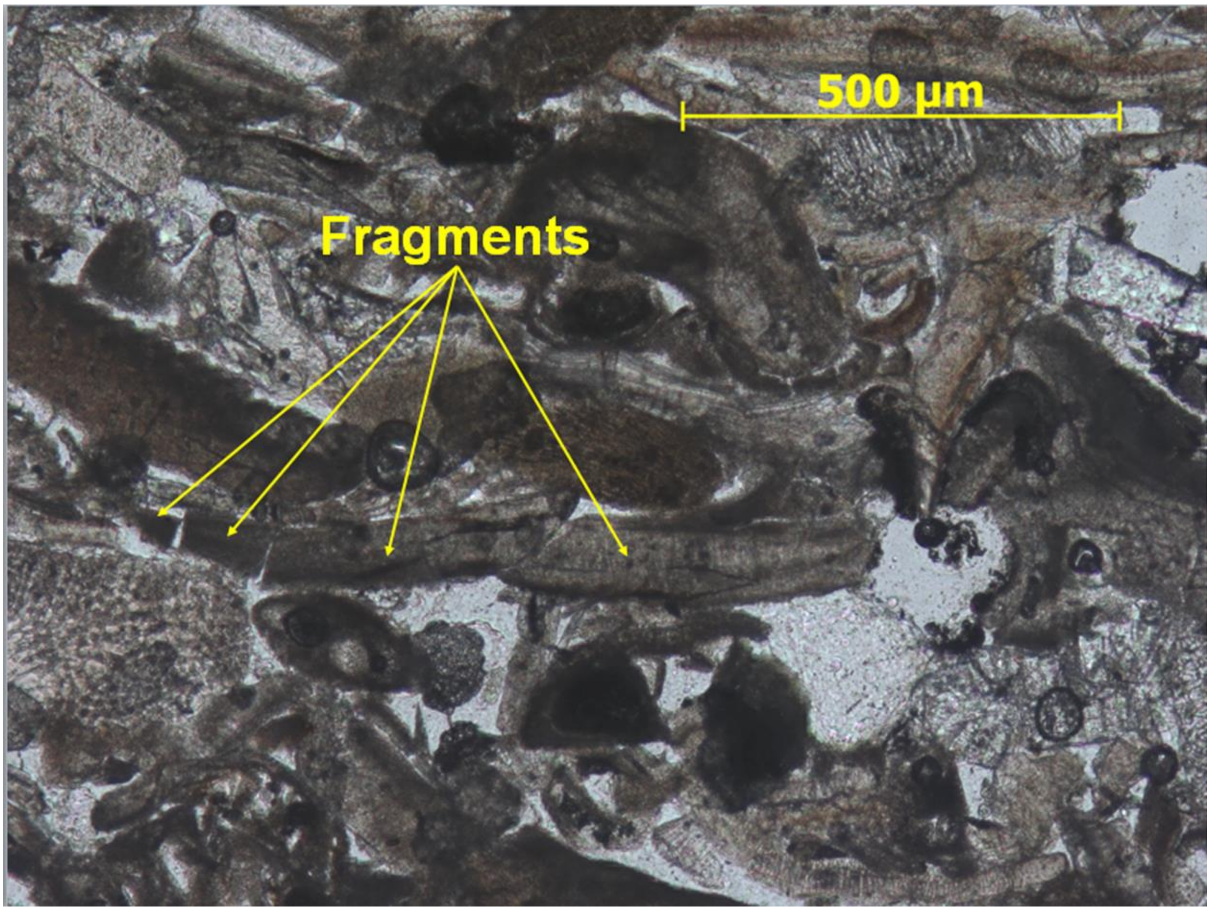

Fig. 21 Example of fragments of particle which are confined to their initial position (redrawn from Bandini and Coop, 2011).